Revised manuscript submitted for publication in

Environmental Science and Technology

December 12 2017

Thallium Adsorption onto Illite

Silvan Wick[1,2], Bart Baeyens[3], Maria Marques Fernandes[3] and Andreas Voegelin[1*]

[1]Eawag, Swiss Federal Institute of Aquatic Science and Technology, Überlandstrasse 133, CH-8600 Dübendorf, Switzerland.

[2]Institute of Biogeochemistry and Pollutant Dynamics, ETH Zürich, CH-8092 Zürich, Switzerland.

[3]Paul Scherrer Institute, CH-5232 Villigen PSI, Switzerland.

[*]corresponding author, E-mail: andreas.voegelin@eawag.ch, phone: +41 58 765 54 70, fax: +41 58 765 58 02.

Abstract

We investigated the adsorption of Tl^+ onto purified Illite du Puy (IdP). Distribution coefficients (K_d) for trace Tl adsorption from pH 2.5 to 11 indicated a moderate pH-dependence. Adsorption isotherms measured at Tl^+ concentrations from 10^{-9} to 10^{-2} M at near-neutral pH on illite saturated with Na^+ (100 mM), K^+ (1 and 10 mM), NH_4^+ (10 mM) or Ca^{2+} (5 mM) revealed a high adsorption affinity of Tl^+ in Na^+- and Ca^{2+}-electrolytes and strong competition with K^+ and NH_4^+. Cation exchange selectivity coefficients for Tl^+ with respect to Na^+, K^+, NH_4^+, and Ca^{2+} were derived using a 3-site sorption model. They confirmed the strong adsorption of Tl^+ at the frayed edges of illite, with Tl selectivity coefficients between those reported for Rb^+ and Cs^+. X-ray absorption spectra of Tl adsorbed onto Na-exchanged IdP indicated a shift from adsorption of (dehydrated) Tl^+ at the frayed edges at low loadings to adsorption of (hydrated) Tl^+ on planar sites at the highest loadings. Our results suggest that illite is an important adsorbent for Tl in soils and sediments, owing to the often high abundance and the stability of illite relative to other potential adsorbents and the selective nature of Tl^+ uptake by illite.

Introduction

Thallium (Tl) is a highly toxic trace element. It occurs in the environment predominantly as monovalent Tl^{I} and to a lesser extent as trivalent Tl^{III}.[1, 2] Since the ionic radius of Tl^{+} (1.70 Å for 12-fold coordination) is similar to the ionic radius of K^{+} (1.64 Å),[3] Tl^{I} can substitute K^{+} in K-bearing rock-forming minerals such as K-feldspars or micas,[1, 4, 5] but is also found in rare minerals such as dorallcharite ($Tl_{0.8}K_{0.2}Fe_3(SO_4)_2(OH)_6$)[6] and lanmuchangite ($TlAl(SO_4)_2 \cdot 12H_2O$).[7] Tl^{III} occurs in water as strongly hydrolysing aqua cation Tl^{3+},[1] forms poorly soluble avicennite (Tl_2O_3)[8] and can be stabilized in Mn-oxides.[9, 10]

Typical Tl contents in soils and sediments range between 0.1-1 mg/kg.[11] High geogenic Tl contents of up to several thousand mg/kg may be found in soils formed on rocks hosting Tl-rich mineralizations.[12, 13] Anthropogenic Tl contamination can result from cement production,[14] metal mining and smelting[15, 16] or coal burning.[2, 17] Because Tl^{+} is relatively soluble, it may be leached into the groundwater or taken up by plants and, via the food chain, may also pose a threat for human health.[18, 19] In soils and sediments, the solubility of Tl is controlled by the stability of Tl-bearing minerals and adsorption processes. Based on the geochemical association of Tl with micas and Mn-oxides,[4, 5, 20] micaceous phyllosilicates such as illite and the phyllomanganate birnessite have long been assumed to be key adsorbents for Tl in soils and sediments.[1, 4, 16, 21-24] This assumption has been corroborated by a recent spectroscopic study on the speciation of Tl in a geogenically Tl-rich soil, which documented the occurrence of Tl^{III} in soil Mn-concretions and confirmed the importance of Tl^{I} sequestration by illite.[12]

Illite is a 2:1 type clay mineral with a basal spacing of 10 Å whose layers are held together by dehydrated K^{+} in the interlayers. Illite in soils may form by the weathering of muscovite.or may be inherited from sedimentary parent material.[25] Replacement of K^{+} at the edges of illite by larger and strongly hydrated cations like Ca^{2+} leads to an expansion of the interlayer spacing to 14 Å within the so-called frayed edge zone.[26, 27] The frayed edges of illite are known to have a very high adsorption selectivity for the weakly hydrated alkali metal cations K^{+}, Rb^{+}, and Cs^{+}

and for NH_4^+. The adsorption of these cations onto illite has been extensively studied with respect to the availability of the nutrients K^+ and NH_4^+ [28, 29] and the retention of the radionuclide ^{137}Cs in soils contaminated from nuclear accidents or in potential host rocks for radioactive waste storage.[25, 26, 29-33] To describe the adsorption of Cs^+ by illite in the presence of competing cations, a multi-site cation exchange model was developed by Brouwer et al. (1983)[34] and generalised by Bradbury and Baeyens (2000)[35] based on three types of cation exchange sites: (i) frayed edge sites (FES) with a very low adsorption capacity (0.25% of the cation exchange capacity (CEC) of illite) but very high affinity, (ii) type-II sites (T2S) with an intermediate affinity and relatively high adsorption capacity (20% of CEC) and (iii) planar sites (PS) on the basal surfaces of illite with a low limited selectivity but high capacity (~80% of CEC). Over time, cations adsorbed to FES can diffuse into the interlayer and replace K^+, leading to their fixation in the illite structure, as observed for Cs^+.[26]

Because of the similarities in dehydration energy and ionic radius between Tl^+ and K^+ and the occurrence of elevated concentrations of Tl in K-rich minerals including micas, Tl has been postulated to be effectively taken up by illite (or, more generally, micaceous clay minerals) in soils and sediments.[1, 4, 12, 16, 21-24, 36] However, the adsorption of Tl^+ by illite has not been studied to date and cation exchange selectivity coefficients are lacking. In this study, we therefore investigated the cation exchange selectivity of Tl^+ on purified homoionic Na-, K-, NH_4- and Ca-illite. We determined the pH-dependence of Tl^+ adsorption at trace concentration and the concentration-dependence at near-neutral pH. From the adsorption isotherms, cation exchange selectivity coefficients were derived based on the generalised 3-site Cs^+ sorption model for illite. X-ray near edge structure (XANES) spectra at the Tl L_{III}-edge were collected on Na-illite with different Tl^+ loadings to gain insight into the mechanism of Tl^+ uptake.

Materials and Methods

Illite du Puy. The illite used for this work has been collected near Le Puy-en-Velay (France) and has previously been used in adsorption studies with different trace metals.[37-39] Purified and conditioned illite du Puy (IdP) suspensions used for the present work were prepared from the same illite source material and following the same procedure as described in detail in previous work.[37] In a first step, IdP was conditioned to homoionic Na^+ form (100 mM NaCl). Using the dialysis technique,[37] initial Na-IdP suspensions were brought to Na^+, K^+, NH_4^+ and Ca^{2+} forms with different background electrolyte concentrations: Na-IdP (in 100 mM $NaNO_3$), K-IdP (in 1 and 10 mM KNO_3), Ca-IdP (in 5 mM $Ca(NO_3)_2$) and NH_4-IdP (in 10 mM NH_4NO_3).

The purified IdP has been reported to mineralogically consist of 88% illite and 12% sanidine.[37] The small sanidine fraction was considered to be non-reactive with respect to Tl^+ adsorption. A N_2-BET surface area of 103 m^2/g has been determined for purified IdP used in this study, in good agreement with a reported N_2-BET surface area of 97 m^2/g.[37] The elemental composition of the purified IdP (48.4% SiO_2, 20.4% Al_2O_3, 7.6% Fe_2O_3, 6.7% K_2O, 3.9% MgO, 0.1% CaO and 0.9% Na_2O) conforms with the compositional formula $[Si_{6.98}Al_{1.02}O_{20}(OH)_4][Al_{2.44}Fe^{III}_{0.82}Mg_{0.84}][Ca_{0.02}Na_{0.24}K_{1.24}]$ proposed by Poinssot et al. (1999)[40] for another batch of Illite du Puy and with the description of Illite du Puy given by van Olphen and Fripiat (1979).[41] Using the Cs isotope dilution technique[42] with ^{204}Tl instead of ^{137}Cs, a Tl-CEC of 0.260 eq/kg was determined for one of the purified IdP batches used in this study, in excellent agreement with the Cs-CEC of 0.263 eq/kg of the respective batch.

General setup of adsorption experiments. Batch adsorption experiments with homoionic IdP suspensions were conducted as a function of solution pH and Tl concentration in different background electrolyte (see Table S1 for an overview of the experimental conditions). All experiments were carried out in 40 mL polypropylene centrifuge tubes (Beckman Coulter). Stable $^{203/205}Tl$ stock solutions were prepared from $TlNO_3$ in the required

background electrolyte and were labelled with radioactive ^{204}Tl (β-emitter; $T_{1/2}$ = 3.78 years; provided by RC TRITEC AG (Teufen, Switzerland); ICP-MS analysis of the tracer solution (0.6 MBq/g): 3.7 % ^{204}Tl, 94.3 % ^{203}Tl and 2 % ^{205}Tl based on ICP-MS analysis). The background electrolyte was spiked with the desired total Tl concentration, and the pH of the solution was adjusted by either HNO_3 or NaOH additions or by using organic pH buffers. Homoionic IdP suspensions were added to obtain the optimal final adsorbent concentrations, depending on the expected extent of Tl uptake. Subsequently, the tubes were closed and shaken end-over-end at room temperature. Based on preliminary experiments on the kinetics of Tl^+ uptake by IdP (details in supporting information; Figure S1), a reaction time of 14 days was used for the experiments described below. After reaction, phase separation was carried out by ultracentrifugation (1 h at 108,000 g (max), Beckman Coulter Avanti™ J30i High-Performance Centrifuge). Two 5 mL aliquots of the supernatant were radio-assayed for the remaining ^{204}Tl activity using a liquid scintillation counter (Packard Tri-Carb 2750 TRILL) and the average of these two independent determinations of remaining activity was taken as one experimental data point. The pH was measured immediately after phase separation in the remaining supernatant. From the decrease in ^{204}Tl activity and the known total Tl concentration ($C_{Tl,init}$, [mol/L]), the final dissolved Tl concentration in the supernatant (C_{Tl}, [mol/L]) was derived. From the decrease in dissolved Tl during reaction, the suspension volume (V_{batch}, [L]) and the mass of illite (m_{IdP}, [kg]), the amount of adsorbed Tl (Q_{Tl}, [mol/kg]) was obtained. Distribution coefficients K_d (in [L/kg]) describing the ratio between dissolved Tl and adsorbed Tl were calculated according to Eq. 1:

$$K_d = \frac{Q_{Tl}}{C_{Tl}} = \frac{(C_{Tl,init} - C_{Tl})}{C_{Tl}} \times \frac{V_{batch}}{m_{IdP}} \quad \text{(Eq. 1)}$$

Each experiment was run in duplicate and the values were treated as independent data points.

pH-dependent adsorption. pH adsorption edges were measured on Na-IdP (100 mM NaCl) and K-IdP (10 and 100 mM KNO_3) in the pH range from ~2.5 to ~11.0. Total initial Tl

concentration, i.e., carrier $^{203/205}Tl$ and tracer ^{204}Tl, was 10^{-8} M. First, the Tl solution was added to the 40 mL centrifuge tubes. Subsequently, the pH was adjusted by either adding 0.1 M HNO_3 (Merck Titrisol®, for pH 4.0 to 5.0), 1 M HNO_3 (Merck Titrisol®, for pH 2.5 to 3.9), 0.1 M NaOH (Merck Titrisol®, for pH 10.0 to 11.0) or 5 mL of pre-prepared organic buffer solutions (for pH 5.3 to 6.8: 0.015 M MES (2-(*N*-morpholino)ethanesulfonic acid); for pH 6.9 to 7.8: 0.015 M MOPS (3-(*N*-morpholino)propanesulfonic acid); for pH 7.9 to 8.6: 0.015 M TRIS (Tris-(hydroxymethyl)aminomethane); for pH 8.7 to 9.9: 0.015 M CHES (2-(cyclohexylamino)ethanesulfonic acid)). Finally, the IdP-suspension was added to achieve an IdP concentration of 2 g/L.

Concentration-dependent adsorption. Adsorption isotherms were measured on Na-IdP (100 mM NaCl (low Tl concentrations) or $NaNO_3$ (high Tl concentrations; to avoid precipitation of TlCl)), K-IdP (1 and 10 mM KNO_3), Ca-IdP (5 mM $Ca(NO_3)_2$) and NH_4-IdP (10 mM NH_4NO_3) for total Tl concentrations from 10^{-9} to 10^{-2} M. The solutions with different Tl concentrations were obtained by diluting a 10^{-2} M $TlNO_3$ stock solution to different levels. The resulting solutions were labelled separately with ^{204}Tl. The pH of each Tl solution was adjusted to ~7.0 using 0.1 M NaOH or 0.1 M HNO_3 (both Merck Titrisol®). The solutions were pipetted in the 40 mL centrifuge tubes, followed by the addition of IdP-suspension to obtain an IdP concentration of 0.7 to 3.8 g/L. Final pH values after equilibration ranged between 6.1 and 6.9 (see Table S1).

Adsorption modeling. All adsorption isotherm data (5 isotherms; 230 data points) were used to derive cation exchange selectivity coefficients for Tl^+-Na^+, Tl^+-K^+, Tl^+-NH_4^+ and Tl^+-Ca^{2+} exchange based on the generalised 3-site cation exchange model for Cs^+ adsorption onto illite of Bradbury and Baeyens (2000),[35] i.e., based on the respective site types and fractions. Cation exchange was treated according to the convention of Gaines and Thomas (1953)[43] (i.e., assuming the activity of adsorbed cations to correspond to their equivalent charge fraction, Equations 2-4):

159 $$A^{n+} + \frac{n}{m} BX_m = AX_n + B^{m+} \quad \text{(Eq. 2)}$$

160 $$K_A^B = \frac{(a_{A^{n+}})^m \times (N_{BX_m})^n}{(N_{AX_n})^m \times (a_{B^{m+}})^n} \quad \text{(Eq. 3)}$$

161 $$N_{AX_n} = \frac{n \times Q_{AX_n}}{Q_{tot,X}} \quad N_{BX_m} = \frac{m \times Q_{BX_m}}{Q_{tot,X}} \quad \text{(Eq. 4)}$$

162 where A and B represent cations with charges n and m respectively, AX_n and BX_m the
163 respective cations bound to the exchange site(s) X, K^B_A the cation exchange selectivity
164 coefficient, a_{An+} and a_{Bm+} the activity of the free cations in solution (in [mol/L]), N_A and N_B
165 the equivalent fractions of the exchangeable bound cations, Q_{AXn} and Q_{BXm} the amounts of
166 the cations A or B bound to site X (in [mol/kg]) and $Q_{tot,X}$ the total concentration of site X
167 (in [eq/kg]; X representing FES, T2S and PS).

168 The model was implemented in the geochemical equilibrium code PhreeqC using the
169 thermodynamic database Minteq.V4 and the Davies equation for the calculation of activity
170 coefficients.[44] For Tl^I, only the stability constants of the aqueous complexes TlCl, $TlCl_2^-$ and
171 $TlNO_3$ were included; oxidation of Tl^I to Tl^{III} and precipitation of Tl-bearing phases were
172 excluded. Similarly, only NH_4^+ and NH_3 were included as dissolved N^{-III} species, and oxidation
173 of N^{-III}, formation of any solution complexes or precipitation of solids was excluded. For
174 parameter refinement, the PhreeqC model was set up in the software code PhreePlot,[45] using
175 the non-linear least squares (modified Levenberg-Marquardt) algorithm to obtain optimized
176 parameters and their uncertainty. For parameter refinement, the sum of the squared residuals
177 between experimental and calculated log K_d values was minimized, based on the total
178 concentrations of Tl^+, Na^+, K^+, NH_4^+, Ca^{2+}, Cl^-, and NO_3^- and the mass of homoionic illite in
179 the suspensions. The fractions of FES (0.25% of CEC), T2S (20% of CEC) and PS (79.75% of
180 CEC) on illite from the generalised 3-site Cs^+ sorption model,[35] and the experimental Tl-CEC
181 (0.260 eq/kg) were used to calculate the individual site capacities, which were treated as non-

adjustable parameters in the model ($Q_{tot,FES}$ = 0.00065 eq/kg; $Q_{tot,T2S}$ = 0.05200 eq/kg; $Q_{tot,PS}$ = 0.20735 eq/kg).

Tl L_{III}-edge XANES spectroscopy. For XANES analyses at the Tl L_{III}-edge, Tl was adsorbed to Na-IdP at Tl loadings from 2.5×10^{-4} to 2.4×10^{-1} mol/kg (50 to 49'000 mg/kg) at background NaCl concentrations of 100 mM (2.5×10^{-4} to 1.9×10^{-2} mol/kg), 95 mM (5.9×10^{-2} mol/kg) or 12 mM (2.4×10^{-1} mol/kg). After the 14-days reaction time, the Tl loaded illite was separated by ultra-centrifugation and supernatant was decanted. The resulting wet paste was filled in acrylic glass sample holders covered with Kapton® tape. Based on a water content of the illite pastes of ~50% (by weight; after centrifugation), dissolved Tl was estimated to correspond to ~3% of the total Tl in the most concentrated sample and to be insignificant in all other samples. A reference spectrum was collected on a 10 mM $TlNO_3$ solution. The XANES spectra were recorded at the SuperXAS beamline (Swiss Light Source, PSI, Switzerland) at room temperature in fluorescence mode using a 5-element silicon drift detector. For data extraction and analysis, the software code Athena was used.[46]

Results and Discussion

Trace Tl^+ adsorption from pH ~2.5 to ~11.0. Distribution coefficients (K_d) for trace Tl^+ adsorption from pH ~2.5 to ~11.0 in 100 mM NaCl, 10 mM and 100 mM KNO_3 background electrolyte are shown in Figure 1A. From 100 mM Na^+ to 10 mM K^+ electrolyte, a pronounced decrease in K_d values by about 1.5 log units can be observed over the entire pH range, indicating that K^+ much more strongly interferes with trace Tl^+ uptake than Na^+. K_d values further decrease by about one order of magnitude when the K^+ concentration increases from 10 to 100 mM. The constant decrease of the log K_d values over the probed pH range when the background electrolyte was varied from 100 mM Na^+ over 10 mM K^+ to 100 mM K^+ clearly points to cation exchange as the dominant adsorption process over the probed pH range. The data further suggested that oxidation of Tl^+ to poorly soluble or strongly binding Tl^{3+} did not detectably

contribute to Tl removal from solution, since both Tl^{+} oxidation and Tl^{3+} precipitation or adsorption would strongly depend on solution pH rather than the type or concentration of the background electrolyte cation.

From pH ~2.5 to ~11.0, K_d values in all three background electrolytes increased regularly by up to 1.3 log units. In the acidic region a smooth gradual decrease of the log K_d with decreasing pH cannot be explained by proton competition on exchange sites alone, because proton competition is only relevant at pH values ≤ 4 and would lead to a steep decrease in log K_d with further decreasing pH (as seen in model calculations for pH-dependent Cs^{+} uptake by illite).[40] Specific adsorption of Tl^{+} at the variably protonated surface hydroxyl groups at the broken bond and edge sites (not FES) of illite platelets could contribute to the more pronounced increase of the adsorption affinity of Tl^{+} at alkaline pH.[37] Based on the relationship between the hydrolysis constants of metal cations and their adsorption constants for coordination at illite edge sites reported in previous work[37, 47] and considering the pK_1 of Tl^{+} of 13.2, adsorption of Tl^{+} onto these sites is expected to be weak at acidic to slightly alkaline pH values, but could become relevant at pH > 10. Other factors that may contribute to increasing log K_d values with increasing pH could include changes in illite surface charge and structure. Finally, illite dissolution at acidic and alkaline pH could affect Tl adsorption, but was expected to be of minor relevance, considering that only 0.1% Illite du Puy has been reported to dissolve within 7 days at pH 3.0[40] and that dissolution rates at pH 4-10 are lower than at pH 3.[48] Although the processes responsible for the observed pH-dependence of Tl^{+} adsorption could not be identified in this study, it is important to note that the log K_d values in all three electrolytes vary by only ~0.3 from pH 6 to 8, i.e., that the pH-dependence of Tl^{+} adsorption onto illite at near neutral pH is weak.

Tl^{+} adsorption isotherms in different background electrolytes. In Figure 1B, the adsorption isotherms of Tl^{+} onto Na-IdP (100 mM NaCl or $NaNO_3$) and K-IdP (1 and 10 mM KNO_3) are shown. The comparison of the adsorption isotherms in 100 mM Na^{+} and in 10 mM

K^+ clearly demonstrate that K^+ effectively reduces Tl^+ uptake at low Tl concentrations (< 10^{-4} M) where specific uptake mechanisms are expected to prevail (Figure 1B). Only at the highest dissolved Tl concentrations, where cation exchange is expected to take place on PS, log K_d values in the presence of 100 mM Na^+ are lower than in the presence of 10 mM K^+. A 10-fold decrease in the K^+ concentration from 10 to 1 mM leads to an increase of about one log unit in Tl adsorption, in line with differences in pH-dependent adsorption in different background electrolytes, again pointing to a cation exchange mechanism as the dominant uptake process even at the lowest Tl concentrations.

The slope of the adsorption isotherm in 100 mM Na^+ electrolyte is below unity, indicating that there are at least two different adsorption sites with different capacities and affinities accessible to Tl^+. The increase in Tl^+ adsorption affinity with decreasing concentration and loading points to the presence of high affinity sites with limited adsorption capacity, where Na^+ is not strongly competitive. A very similar adsorption isotherm is observed in 5 mM $Ca(NO_3)_2$ (Figure 1C), in line with the known low affinity of alkaline earth cations for uptake at frayed edge sites.[34, 49] The slope near unity of the adsorption isotherm in 1 and 10 mM K^+, on the other hand, indicates that K^+ effectively reduces high-affinity Tl^+ adsorption. A nearly identical adsorption isotherm as in 10 mM KNO_3 electrolyte was measured in 10 mM NH_4NO_3 electrolyte (Figure 1C), indicating that K^+ and NH_4^+ affect the extent of Tl^+ adsorption in a very similar way.

Cation exchange modeling. Cation exchange selectivity coefficients for Tl^+ exchange equilibria with respect to Na^+, K^+, NH_4^+, Ca^{2+}, were derived by fitting the five experimental adsorption isotherms (Figure 1BC) based on the site types and fractions from the generalised 3-site cation exchange model for Cs^+ onto illite. Preliminary fits indicated a very high negative correlation between the Tl^+-K^+ selectivity coefficients on T2S and PS and the refined coefficients were nearly identical. Therefore, the two cation exchange coefficients were defined to be equal to reduce the associated parameter uncertainty. The optimized Tl-X selectivity

coefficients are reported in Table 1, together with resulting cation exchange coefficients for major cations and for Cs^+ and Rb^+ from the generalised 3-site Cs^+ sorption model of Bradbury and Baeyens (2000).[35] The modeled log K_d values as a function of dissolved Tl concentrations are shown in Figure 2A-E, the modeled Tl adsorption isotherms in Figure S2 in the supplementary information.

Comparison of the Tl-Na or Tl-K exchange selectivity coefficients on FES and T2S with the Cs-Na and Rb-Na or Cs-K and Rb-K exchange coefficients of the generalised 3-site sorption model (Table 1) consistently indicate that, overall, Tl^+ adsorption onto illite exhibits an affinity between the affinities of Cs^+ and Rb^+. In Table 2, the Tl-X exchange coefficients on FES and T2S are compared to the effective ionic radii (for 12-fold coordination) and molar Gibbs hydration energies of the respective cation. The very high selectivity of Tl^+ with respect to Na^+ and Ca^{2+} on FES can be linked to the unsuitable ionic radii of Na^+ and Ca^{2+} and their (much) more negative hydration energies. With respect to the cations K^+, NH_4^+, Rb^+ and Cs^+, a consistent decrease in selectivity can be observed as a function of both increasing ionic radius and less negative hydration energy (higher tendency to dehydrate). The Tl^+ cation does not closely follow this trend with a cation exchange selectivity coefficient between Cs^+ and Rb^+, an ionic radius between NH_4^+ and Rb^+ and a hydration energy similar to K^+ (Table 2). This may be due to the fact that Tl is a post-transition metal in the boron group and not an alkali metal and that, consequently, the electronic configuration of the Tl^+ cation with a lone electron pair is markedly different from the cations K^+, Rb^+ and Cs^+.

From the Tl-X exchange coefficients, also the cation exchange selectivity coefficients of the major cations K^+, Ca^{2+} and NH_4^+ versus Na^+ were derived (Table 1). For PS, it was found that the respective major cation exchange selectivity coefficients were close to K^+-Na^+, NH_4^+-Na^+ and Ca^{2+}-Na^+ selectivity coefficients reported for montmorillonite (log $K^{K}_{Na} = 0.4\pm0.2$; log $K^{NH4}_{Na} = 0.7\pm0.1$; log $K^{Ca}_{Na} = 0.8\pm0.4$; derived from the compilation of cation exchange selectivity coefficients in ref. [50]), which may be taken as proxy for PS of illite. The major cation

285 exchange coefficients for T2S and FES reflect a much stronger selectivity of K^+ and NH_4^+ than
286 Na^+ and Ca^{2+} at the frayed edges of illite.

287 According to the model calculations, Tl uptake onto Na- and Ca-IdP is dominated by FES
288 for Tl concentrations up to almost 10^{-7} M, and by T2S for concentrations up to nearly 10^{-3} M
289 (Figure 2). In the 1 mM and especially the 10 mM K^+ electrolyte (K-IdP), in contrast, Tl^+
290 adsorption onto FES was substantially reduced, and Tl^+ adsorption to PS contributed
291 significantly to total Tl uptake even at lowest Tl concentrations. For Tl^+ adsorption in 10 mM
292 NH_4^+ electrolyte (NH_4-IdP), the fit returned site contributions that markedly varied from the 10
293 mM K^+ electrolyte, with a dominance of T2S over a wide Tl^+ concentration range. The
294 discrepancy between the 10 mM K^+ and 10 mM NH_4^+ electrolytes in terms of adsorption site
295 relevance may point to true differences in the impact of these ions on the preferential way of
296 Tl^+ uptake, but may also just reflect that the respective fits were poorly constrained as two sites
297 would have been sufficient to satisfactorily describe the respective log K_d curves.

298 **Tl L_{III}-edge XANES spectra.** Tl L_{III}-edge XANES spectra collected on Na-IdP with Tl
299 loadings from 2.5×10^{-4} to 2.4×10^{-1} mol/kg Tl (samples #1 to #5; 50 to 49'000 mg/kg Tl) are
300 shown in Figure 3, together with the modeled distribution of Tl over the three types of exchange
301 sites considered in the model and results from the analysis of the sample spectra by spectral
302 comparison or linear combination fitting (LCF). According to the model calculations, the Tl
303 was mainly adsorbed to FES in sample #1 (2.5×10^{-4} mol/kg Tl), to T2S in sample #3 (1.9×10^{-2}
304 mol/kg Tl), and to PS in sample #5 (2.4×10^{-1} mol/kg Tl) (Figure 3B).

305 From sample #1 (mainly Tl on FES) to sample #3 (mainly Tl on T2S), no marked spectral
306 change was observed. Indeed, the spectra of samples #1 and #2 could be perfectly matched with
307 the spectrum of sample #3 (Figure 3A), suggesting that Tl coordination did not detectably vary
308 over the respective range in Tl loading. In combination with the model calculations, this
309 spectroscopic finding suggests that FES and T2S of the 3-site sorption model serve to describe
310 the decreasing adsorption affinity of dehydrated Tl^+ bound at the frayed edges of illite platelets

311 with increasing Tl loading, in line with the interpretation of these model sites in earlier work
312 on the uptake of Cs^+ and Rb^+ by illite.[34, 49]

313 From sample #3 (mainly Tl on T2S) to sample #5 (mainly Tl on PS), on the other hand,
314 a clear shift in the spectra was observed. LCF analysis showed that spectra #4 and #5 could be
315 adequately reproduced by linear combinations of the spectra of sample #3 and of hydrated
316 aqueous Tl^+ (Figure 3AC). Assuming that the spectrum of sample #3 represents dehydrated Tl^+
317 adsorbed at the frayed edges of illite and the spectrum of aqueous Tl^+ represents hydrated Tl^+
318 adsorbed on planar sites, the spectral trend was in agreement with the adsorption model that
319 indicated a transition from predominant Tl^+ adsorption at the frayed edges of illite in sample #3
320 to predominant adsorption of Tl^+ at planar sites in sample #5 (Figure 3B). The difference
321 between the modeled fraction of Tl at PS and of LCF-derived fraction of hydrated Tl^+ in sample
322 #5 may be due to various factors, including uncertainties in model calculations or the non-
323 consideration of the potential role of partially dehydrated adsorbed Tl^+ (on PS or at FES) in
324 addition to fully dehydrated and fully hydrated Tl^+ (as inferred for Cs^+ uptake on clay minerals
325 based on XAS results).[51, 52]

326 **Adsorption of Tl^+ onto illite in arable soil porewater.** The adsorption of Tl^+ onto illite
327 was modeled for typical concentrations of Ca^{2+}, Mg^{2+}, Na^+, K^+ and NH_4^+ in the porewater of
328 arable soils (from ref. [53]; details in Table S2; Mg^{2+} assumed to exhibit the same cation exchange
329 behaviour as Ca^{2+}). For average cation concentrations, the modeled log K_d as a function of the
330 dissolved Tl concentration is shown in Figure 2F, together with the contribution of the
331 individual types of sites. The results show that Tl^+ adsorption onto illite in equilibrium with the
332 soil solution was dominated by FES (and T2S) over environmentally relevant ranges in
333 dissolved and adsorbed Tl^+, and that adsorption to PS was of minor importance (Figure 2F).
334 This was also true if Tl^+ adsorption onto illite was modeled for the lower or upper bounds of
335 common cation concentrations (not shown). Figure 4 shows the modeled adsorption of Tl^+ onto
336 illite from arable soil porewater with average cation concentrations (thick gray lines) as well as

for lower and upper bounds of common concentration of Ca^{2+}, Mg^{2+}, Na^{+}, K^{+} and NH_4^{+} (light gray area). The calculations reveal that the log K_d (K_d in units of [L/kg]) for Tl^{+} adsorption onto illite at dissolved concentrations $<10^{-7}$ M varies between 2.9 and 3.9. Further calculations with low Ca^{2+}, Mg^{2+} and Na^{+} and high K^{+} and NH_4^{+} concentrations and vice versa (not shown) indicated that the trace Tl^{+} adsorption isotherms strongly dependent on the concentrations of K^{+} and NH_4^{+} which compete for adsorption onto FES and T2S, but much less on the concentrations of Ca^{2+} and Mg^{2+}. However, these alkaline earth cations are relevant as they limit Tl^{+} adsorption onto PS.

Comparison of Tl^{+} adsorption onto illite and other adsorbents. In Figure 4, published data for Tl^{+} adsorption onto humic acid,[54] ferrihydrite[15] and hexagonal birnessites[55-57] are compared to the predicted adsorption of Tl^{+} onto illite in arable soil porewater. Noting that the sorption experiments with ferrihydrite and humic acids were performed in Na^{+} electrolytes and do not reflect the effects of more competitively adsorbing cations, the comparison suggests that humic acids and Fe-oxides may also be important adsorbents for Tl in specific environments, e.g., humic acids in forest topsoils for which enhanced levels of labile Tl have been attributed to Tl adsorption onto soil organic matter,[58] or ferrihydrite in environments affected by acid mine drainage.[15]

Consistent data for Tl^{+} adsorption onto hexagonal birnessite, a synthetic proxy of biogenic Mn oxides,[59] was compiled from three studies[55-57] (Fig. 4). The very strong uptake of Tl^{+} by hexagonal birnessite at low dissolved Tl^{+} concentrations has been attributed to oxidative Tl complexation on vacancy sites in octahedral MnO_2 sheets (characteristic of hexagonal birnessite).[9, 10] The strong decrease in the log K_d with increasing Tl loading points to a shift to less specific and probably non-oxidative sorption mechanisms after saturation of vacancy sites, as previously inferred from trends in Tl isotope fractionation.[57] The much higher log K_d of Tl bound to hexagonal birnessite than illite at low dissolved Tl^{+} concentrations allows to rationalize the high enrichment of Tl in marine ferromanganese nodules relative to pelagic

clays,[60] or the observation that addition of 0.5% (by weight) hexagonal birnessite to two soils spiked with 5 mg/kg Tl resulted in a depletion of the exchangeable Tl fraction and reduced Tl uptake by mustard, whereas addition of 1.5% illite did not show such an effect.[16] Conversely, the predominant association of Tl with illite in a geogenically Tl-rich soil has partly been attributed to high Tl loadings that exceeded the adsorption capacity of birnessite.[12] More generally, the role of hexagonal birnessite as an adsorbent for Tl in a specific environment, relative to illite and other adsorbents, may be constrained by various factors that are not reflected by the adsorption data shown in Fig. 4, such as the abundance of the respective adsorbents, their chemical stability, and competitive cation uptake. For example, soils typically contain less than 1000 mg/kg Mn[61] and hexagonal birnessite may account for only a fraction of the soil Mn, whereas illite and other micaceous phyllosilicates often represent a major soil component. In addition, many trace elements that are typically more abundant than Tl such as Ba, Co, Ni, Cu, Zn or Pb also strongly adsorb onto hexagonal birnessite[59, 62, 63] and may limit Tl uptake. Over time, biogenic hexagonal birnessite can also transform into Mn-oxides with lower adsorption capacity.[64] Finally, Mn-oxides are susceptible to reductive dissolution under anoxic conditions, which constrains their relevance and impact in periodically and permanently reducing environments.

Implications of Tl^+ adsorption onto illite and other micaceous phyllosilicates. This study demonstrated that Tl^+ strongly adsorbs onto illite with an adsorption affinity between Rb^+ and Cs^+ and that Tl^+ uptake can be described using a 3-site cation exchange model previously developed to describe the competitive adsorption of Cs^+, Rb^+, NH_4^+ and K^+ onto illite.[35] For Cs^+, high adsorption affinities at low loadings have also been documented for other micaceous phyllosilicates, most importantly (weathered) biotite and muscovite[33, 65] and (hydroxy-interlayered) vermiculite,[29, 66-68] but also illite-interstratified smectite.[69] Considering the results from this study, we postulate that Tl^+ will equally adsorb onto these minerals with a cation exchange selectivity between those of Rb^+ and Cs^+ (Table 2).

389 Studies with Cs^+ indicated that adsorption onto illite occurs within hours to days, but that
390 desorption kinetics can be slow and that periods of months to even years may be necessary to
391 reach desorption equilibrium, depending also on the concentrations of K^+ and NH_4^+ that may
392 cause a collapse of the frayed edges and thereby inhibit desorption.[70-73] Assuming that Tl^+
393 behaves similarly, slow desorption kinetics may limit short-term Tl^+ release, for example during
394 rapid soil infiltration during rain events, but equilibrium conditions can be assumed over longer
395 reaction times and in less dynamic environments. Over longer periods of time, Tl^+ adsorbed at
396 the FES of illite could also diffuse into the interlayer and become structurally fixed, as has been
397 observed for Cs^+ and proposed for geogenic Tl in soils.[12, 58] On the other hand, for a soil
398 containing 12% illite and contaminated by the emissions of a cement plant, a high-fraction
399 (~70%) of the total soil Tl (3 mg/kg) was found to be present in exchangeable form and was
400 also available for plant uptake, suggesting that Tl fixation in micaceous clay minerals over the
401 time of soil contamination (or slow desorption kinetics) did not substantially limit Tl release.
402 As our results show, the amount of Tl^+ bound at the frayed edges of illite strongly depends
403 on adsorption competition with K^+ and NH_4^+. Thus, processes that can lead to an increase of
404 these cations in solution, such as fertilization of soils with K^+ or NH_4^+ or reduction of NO_3^- to
405 NH_4^+ in flooded soils and sediments may strongly impact on Tl^+ solubility. The cation exchange
406 model for Tl^+ adsorption onto illite derived in this study provides a solid basis to estimate such
407 effects and, more generally, to assess the effect of Tl^+ adsorption onto illite on the retention and
408 solubility of Tl in soils and sediments.

409 **Acknowledgements**

410 Five anonymous reviewers are acknowledged for their positive and constructive
411 comments on an earlier version of this manuscript. We thank Astrid Schaible and Elmotaz
412 Eltayeb (PSI) for laboratory support. The Swiss Light Source (PSI) is acknowledged for the
413 allocation of beam time, and Olga Safonova and Maarten Nachtegaal (PSI) for support during

data collection at the SuperXAS beamline. This work was financially supported by the Swiss National Science Foundation under contract No. 200021-16236.

Supporting Information

Time-resolved trace Tl adsorption onto Na-exchanged and K-exchanged IdP at different pH values, experimental and modeled adsorption isotherms for Tl^+ adsorption onto illite at near-neutral pH, experimental conditions of pH- and concentration-dependent adsorption experiments, derivation of common concentration of major cations in arable soil porewater and description of Tl^+ adsorption data for various adsorbents derived from the literature. This material is available free of charge via the Internet at http://pubs.acs.org/.

References

1. Nriagu, J. O., *Thallium in the Environment*. John Wiley & Sons, New York: 1998; Vol. 29.
2. John Peter, A. L.; Viraraghavan, T., Thallium: a review of public health and environmental concerns. *Environment International* **2005,** *31*, 493-501.
3. Shannon, R. D., Revised effective ionic radii and systematic studies of interatomic distances in halides and chalcogenides. *Acta Crystallographica A* **1976,** *32*, 751-767.
4. Jović, V., Thallium in rocks, soils, and plants: past progress and future needs. *Neues Jahrbuch für Mineralogie - Abhandlungen* **1993,** *166*, 43-52.
5. Heinrichs, H.; Schulz-Dobrick, B.; Wedepohl, K. H., Terrestrial geochemistry of Cd, Bi, Tl, Zn and Rb. *Geochim. Cosmochim. Acta* **1980,** *44*, 1519-1533.
6. Balič Žunić, T.; Moëlo, Y.; Lončar, Ž.; Micheelsen, H., Dorallcharite, $Tl_{0.8}K_{0.2}Fe_3(SO_4)_2(OH)_6$, a new member of the jarosite-alunite family. *European Journal of Mineralogy* **1994,** *6*, 255-263.
7. Daiyan, C.; Guanxin, W.; Zhenxi, Z.; Yuming, C., Lanmuchangite, a new thallium (hydrous) sulphate from Lanmuchang, Guizhou Province, China. *Chinese Journal of Geochemistry* **2003,** *22*, 185-192.
8. Radtke, A. S.; Dickson, F. W.; Slack, J. F., Occurrence and formation of avicennite, Tl_2O_3, as a secondary mineral at the Carlin gold deposit, Nevada. *Journal of Research of the U.S. Geological Survey* **1978,** *6*, (2), 241-246.
9. Peacock, C. L.; Moon, E. M., Oxidative scavenging of thallium by birnessite: Explanation for thallium enrichment and stable isotope fractionation in marine ferromanganese precipitates. *Geochim. Cosmochim. Acta* **2012,** *84*, 297-313.
10. Bidoglio, G.; Gibson, P. N.; O'Gorman, M.; Roberst, K. J., X-ray absorption spectroscopy investigation on surface redox transformations of thallium and chromium on colloidal mineral oxides. *Geochim. Cosmochim. Acta* **1993,** *57*, 2389-2394.
11. Kabata-Pendias, A., *Trace Elements in Soils and Plants*. 4th ed.; CRC Press: Boca Raton, 2011.

12. Voegelin, A.; Pfenninger, N.; Petrikis, J.; Majzlan, J.; Plötze, M.; Senn, A.-C.; Mangold, S.; Steininger, R.; Göttlicher, J., Thallium speciation and extractability in a thallium- and arsenic-rich soil developed from mineralized carbonate rock. *Environ. Sci. Technol.* **2015,** *49*, 5390-5398.
13. Xiao, T.; Yang, F.; Li, S.; Zheng, B.; Ning, Z., Thallium pollution in China: A geo-environmental perspective. *Science of the Total Environment* **2012,** *421-422*, 51-58.
14. Kersten, M.; Xiao, T.; Kreissig, K.; Brett, A.; Coles, B. J.; Rehkämper, M., Tracing anthropogenic thallium in soil using stable isotope compositions. *Environ. Sci. Technol.* **2014,** *48*, 9030-9036.
15. Casiot, C.; Egal, M.; Bruneel, O.; Verma, N.; Parmentier, M.; Elbaz-Poulichet, F., Predominance of aqueous Tl(I) species in the river system downstream from the abandoned Carnoulès mine (Southern France). *Environ. Sci. Technol.* **2011,** *45*, 2056-2064.
16. Vaněk, A.; Komárek, M.; Vokurková, P.; Mihaljevic, M.; Šebek, O.; Panušková, G.; Chrastný, V.; Drábek, O., Effect of illite and birnessite on thallium retention and bioavailability in contaminated soils. *J. Haz. Mat.* **2011,** *191*, 170-176.
17. Cheam, V.; Garbai, G.; Lechner, J.; Rajkumar, J., Local impacts of coal mines and power plants across Canada. I. Thallium in waters and sediments. *Water Quality Research Journal of Canada* **2000,** *35*, (4), 581-607.
18. Campanella, B.; Onor, M.; D'Ulivo, A.; Giannecchini, R.; D'Orazio, M.; Petrini, R.; Bramanti, E., Human exposure to thallium through tap water: A study from Valdicastello Carducci and Pietrasanta (northern Tuscany, Italy). *Science of the Total Environment* **2016,** *548-549*, 33-42.
19. Xiao, T.; Boyle, D.; Guha, J.; Rouleau, A.; Hong, Y.; Zheng, B., Groundwater-related thallium transfer processes and their impacts on the ecosystem: southwest Guizhou Province, China. *Appl. Geochem.* **2003,** *18*, 675-691.
20. Shaw, D. M., The geochemistry of thallium. *Geochim. Cosmochim. Acta* **1952,** *2*, 118-154.
21. Jacobsen, A. R.; McBride, M. B.; Baveye, P.; Steenhuis, T. S., Environmental factors determining the trace-level sorption of silver and thallium to soils. *Science of the Total Environment* **2005,** *345*, 191-205.
22. Matthews, A. D.; Riley, J. P., The occurrence of thallium in sea water and marine sediments *Chem. Geol.* **1970,** *6*, 149-152.
23. Lehn, H.; Schoer, J., Thallium-transfer from soils to plants: Correlation between chemical form and plant uptake. *Plant and Soil* **1987,** *97*, 253-265.
24. Tremel, A.; Masson, P.; Sterckeman, T.; Baize, D.; Mench, M., Thallium in French agrosystems - I. Thallium contents in arable soils. *Environmental Pollution* **1997,** *95*, (3), 293-302.
25. Meunier, A.; Velde, B., *Illite*. Springer-Verlag: Berlin, Heidelberg, 2004; p 286.
26. Fuller, A. J.; Shaw, S.; Ward, M. B.; Haigh, S. J.; Mosselmans, J. F. W.; Peacock, C. L.; Stackhouse, S.; Dent, A. J.; Trivedi, D.; Burke, I. T., Caesium incorporation and retention in illite interlayers. *Applied Clay Science* **2015,** *108*, 128-134.
27. Jackson, M., Weathering of primary and secondary minerals in soils. **1968,** *4*, 281-292.
28. Bolt, G. H.; Sumner, M. E.; Kamphorst, A., A study of the equilibria between three categories of potassium in an illitic soil. *Soil Sci. Soc. Am. Proc.* **1963,** *27*, 294-299.
29. Sawhney, B. L., Selective sorption and fixation of cations by clay minerals: A review. *Clays Clay Min.* **1972,** *20*, (93-100).

30. Komarneni, S., Cesium sorption by clay-minerals and shales at elevated-temperatures. *Journal of Inorganic and Nuclear Chemistry* **1979,** *41*, (3), 397-400.
31. Komarneni, S.; Roy, D. M., Shale as a radioactive-waste repository - Importance of vermiculite. *Journal of Inorganic and Nuclear Chemistry* **1979,** *41*, (12), 1793-1796.
32. Tamura, T.; Jacobs, D. G., Structural implications in cesium sorption. *Health Phys* **1960,** *2*, (4), 391-398.
33. Zachara, J. M.; Smith, S. C.; Liu, C.; McKinley, J. P.; Serne, R. J.; Gassmann, P. L., Sorption of Cs+ to micaceous subsurface sediments from the Hanford site, USA. *Geochemica et Cosmochimica Acta* **2002,** *66*, 193-211.
34. Brouwer, E.; Baeyens, B.; Maes, A.; Cremers, A., Cesium and rubidium ion equilibria in illite clay. *J. Phys. Chem.* **1983,** *87*, 1213-1219.
35. Bradbury, M. H.; Baeyens, B., A generalised model for the concentration dependent uptake of caesium by argillaceous rocks. *J. Contam. Hydrol.* **2000,** *42*, 141-163.
36. Jacobson, A. R.; McBride, M. B.; Baveye, P.; Steenhuis, T. S., Environmental factors determining the trace-level sorption of silver and thallium to soils. *Science of the Total Environment* **2005,** *345*, 191-205.
37. Bradbury, M. H.; Baeyens, B., Sorption modelling on illite. Part I: Titration measurements and the sorption of Ni, Co, Eu and Sn. *Geochim. Cosmochim. Acta* **2009,** *73*, (4), 990-1003.
38. Bradbury, M. H.; Baeyens, B., Sorption modelling on illite. Part II: Actinide sorption and linear free energy relationships. *Geochim. Cosmochim. Acta* **2009,** *73*, (4), 1004-1013.
39. Schnurr, A.; Marsac, R.; Rabung, T.; Lutzenkirchen, J.; Geckeis, H., Sorption of Cm(III) and Eu(III) onto clay minerals under saline conditions: Batch adsorption, laser-fluorescence spectroscopy and modeling. *Geochim. Cosmochim. Acta* **2015,** *151*, 192-202.
40. Poinssot, C.; Baeyens, B.; Bradbury, M. H., Experimental and modelling studies of caesium sorption on illite. *Geochim. Cosmochim. Acta* **1999,** *63*, (19/20), 3217-3227.
41. van Olphen, H.; Fripiat, J. J., *Data Handbook for Clay Materials and other non-metallic Minerals*. Pergamon: Oxford a.o., 1979; p 346.
42. Baeyens, B.; Bradbury, M. H., Cation exchange capacity measurements on illite using the sodium and cesium isotope dilution technique: Effects of the index cation, electrolyte concentration and competition: Modeling. *Clays Clay Min.* **2004,** *52*, (4), 421-431.
43. Gaines, G. L. J.; Thomas, H. C., Adsorption studies on clay minerals. II: A formulation of the thermodynamics of exchange adsorption. *The Journal of Chemical Physics* **1953,** *21*, 714-718.
44. Parkhurst, D. L.; Appelo, C. A. J. *User's guide to PHREEQC (Version 2) -- a computer program for speciation, batch-reaction, one-dimensional transport, and inverse geochemical calculations*; 99-4259; U.S. Geological Survey: Denver, CO, 1999; p 312.
45. Kinniburgh, D. G.; Cooper, D. M. PhreePlot: Creating graphical output with PHREEQC. http://www.phreeplot.org.
46. Ravel, B.; Newville, M., ATHENA, ARTEMIS, HEPHAESTUS: data analysis for X-ray absorption spectroscopy using IFEFFIT. *J. Synchrotron Rad.* **2005,** *12*, 537-541.
47. Bradbury, M. H.; Baeyens, B.; Geckeis, H.; Rabung, T., Sorption of Eu(III)/Cm(III) on Ca-montmorillonite and Na-illite. Part 2: Surface complexation modelling. *Geochim. Cosmochim. Acta* **2005,** *69*, (23), 5403-5412.
48. Köhler, S. J.; Dufaud, F.; Oelkers, E. H., An experimental study of illite dissolution kinetics as a function of pH from 1.4 to 12.4 and temperature from 5 to 50°C. *Geochim. Cosmochim. Acta* **2003,** *67*, 3583-3594.

49. Benedicto, A.; Missana, T.; Fernández, A. M., Interlayer collapse affects on cesium adsorption onto illite. *Environ. Sci. Technol.* **2014,** *48*, 4909-4915.
50. Bruggenwert, M. G. M.; Kamphorst, A., Survey of experimental information on cation exchange in soil systems. In *Soil Chemistry: B. Physico-Chemical Models*, Bolt, G. H., Ed. Elsevier: Amsterdam, 1979; pp 141-203.
51. Bostick, B. C.; Vairavamurthy, M. A.; Karthikeyan, K. G.; Chorover, J., Cesium adsorption on clay minerals: an EXAFS spectroscopic investigation. *Environ. Sci. Technol.* **2002,** *36*, (12), 2670-2676.
52. Kemner, K. M.; Hunter, D. B.; Bertsch, P. M.; Kirkland, J. P.; Elam, W. T., Determination of site specific binding environments of surface sorbed cesium on clay minerals by Cs-EXAFS. *J Phys IV* **1997,** *7*, (C2), 777-779.
53. Blume, H. P.; Scheffer, F.; Schachtschabel, P., *Scheffer/Schachtschabel Soil Science*. Springer Verlag: Berlin, Heidelberg, 2016; p 618.
54. Liu, J.; Lippold, H.; Wang, J.; Lippmann-Pipke, J.; Chen, Y., Sorption of thallium(I) onto geological materials: Influence of pH and humic matter. *Chemosphere* **2011,** *82*, 866-871.
55. Wan, S.; Ma, M.; Lv, L.; Qian, L.; Xiu, S.; Xue, Y.; Ma, Z., Selective capture of thallium(I) ion from aqueous solutions by amorphous hydrous manganese dioxide. *Chemical Engineering Journal* **2014,** *239*, 200-206.
56. Huangfu, X.; Jiang, J.; Lu, X.; Wang, Y.; Liu, Y.; Pang, S.-Y.; Cheng, H.; Zhang, X. H.; Ma, J., Adsorption and oxidation of thallium(I) by a nanosized manganese dioxide. *Water Air and Soil Pollution* **2015,** *226*, 2272:1-9.
57. Nielsen, S. G.; Wasylenki, L. E.; Rehkämper, M.; Peacock, C. L.; Xue, Z.; Moon, E. M., Towards an understanding of thallium isotope fractionation during adsorption to manganese oxide. *Geochim. Cosmochim. Acta* **2013,** *117*, 252-265.
58. Vaněk, A.; Chrastný, V.; Mihaljevic, M.; Drahota, P.; Grygar, T.; Komárek, M., Lithogenic thallium behavior in soils with different land use. *Journal of Geochemical Exploration* **2009,** *102*, 7-12.
59. Tebo, B. M.; Bargar, J. R.; Clement, B. G.; Dick, G. J.; Murray, K. J.; Parker, D.; Verity, R.; Webb, S. M., Biogenic manganese oxides: Properties and mechanisms of formation. *Annual Review of Earth and Planetary Sciences* **2004,** *32*, 287-328.
60. Flegal, A. R.; Sanudo-Wilhelmy, S., Particulate thallium fluxes in the Northeast Pacific. *Mar. Chem.* **1989,** *28*, 61-75.
61. Salminen, R., *Geochemical Atlas of Europe. Part 1: Background Information, Methodology and Maps*. Geological Survey of Finland: Espoo, 2005; p 526.
62. Manceau, A.; Lanson, B.; Drits, V. A., Structure of heavy metal sorbed birnessite. Part III: Results from powder and polarized extended X-ray absorption fine structure spectroscopy. *Geochim. Cosmochim. Acta* **2002,** *66*, (15), 2639-2663.
63. Peacock, C. L.; Sherman, D. M., Sorption of Ni by birnessite: Equilibrium controls on Ni in seawater. *Chem. Geol.* **2007,** *238*, 94-106.
64. Atkins, A. L.; Shaw, S.; Peacock, C. L., Nucleation and growth of todorokite from birnessite: Implications for trace-metal cycling in marine sediments. *Geochim. Cosmochim. Acta* **2014,** *144*, 109-125.
65. Mukai, H.; Hirose, A.; Motai, S.; Kikuchi, R.; Tanoi, K.; Nakanishi, T. M.; Yaita, T.; Kogure, T., Cesium adsorption/desorption behavior of clay minerals considering actual contamination conditions in Fukushima. *Scientific Reports* **2016,** *6:21543*, 1-7.

66. Zaunbrecher, L. K.; Cygan, R. T.; Elliott, W. C., Molecular models of cesium and rubidium adsorption on weathered micaceous minerals. *J. Phys. Chem. A* **2015,** *119*, 5691−5700.

67. Zaunbrecher, L. K.; Elliott, W. C.; Wampler, J. M.; Perdrial, N.; Kaplan, D. I., Enrichment of cesium and rubidium in weathered micaceous materials at the Savannah river site, South Carolina. *Environmenal Science and Technology* **2015,** *49*, 4226−4234.

68. Fan, Q. H.; Tanaka, M.; Tanaka, K.; Sakaguchi, A.; Takahashi, Y., An EXAFS study on the effects of natural organic matter and the expandability of clay minerals on cesium adsorption and mobility. *Geochim. Cosmochim. Acta* **2014,** *135*, 49-65.

69. Missana, T.; Benedicto, A.; García-Gutiérrez, M.; Alonso, U., Modeling cesium retention onto Na-, K- and Ca-smectite: Effects of ionic strength, exchange and competing cations on the determination of selectivity coefficients. *Geochim. Cosmochim. Acta* **2014,** *128*, 266-277.

70. Durrant, C. B.; Begg, J. D.; Kersting, A. B.; Zavarin, M., Cesium sorption reversibility and kinetics on illite, montmorillonite, and kaolinite. *Science of the Total Environment* **2018,** *610–611*, 511–520.

71. de Koning, A.; Comans, R. N. J., Reversibility of radiocaesium sorption on illite. *Geochim. Cosmochim. Acta* **2004,** *68*, 2815-2823.

72. Comans, R. N. J.; Haller, M.; de Peter, P., Sorption of cesium on illite: Non-equilibrium behaviour and reversibility. *Geochim. Cosmochim. Acta* **1991,** *55*, 433-440.

73. Comans, R. N. J., Kinetics and reversibility of radiocesium sorption on illite and sediments containing illite. In *Mineral-Water Interfacial Reactions: Kinetics and Mechanisms*, Sparks, D. L.; Grundl, T. J., Eds. ACS: 1999.

74. Sidey, V., On the effective ionic radii for ammonium. *Acta Crystallogr B* **2016,** *72*, 626-633.

75. Marcus, Y., Thermodynamics of solvation of ions. 5. Gibbs free-energy of hydration at 298.15 K. *Journal of the Chemical Society - Faraday Transactions* **1991,** *87*, (18), 2995-2999.

Tables

Table 1: Cation exchange selectivity coefficients for Tl^+-Na^+, Tl^+-K^+, Tl^+-NH_4^+ and Tl^+-Ca^{2+} exchange refined from the log K_d of Tl^+ in homoionic Na-illite, K-illite, NH_4-illite and Ca-illite suspensions at near neutral pH (Fig. 2). Values in parentheses indicate numerical fit uncertainty. The selectivity coefficients for major cations were calculated from the Tl-X selectivity coefficients. Cs^+-X and Rb^+-X selectivity coefficients from Bradbury and Baeyens (2000)[35] are shown for comparison.

Site	FES	T2S	PS
Site fractions[a]	0.25% of CEC	20% of CEC	79.75% of CEC
	Tl-X exchange selectivity coefficients derived from Tl isotherms		
$\log K_{Ca}^{Tl}$	12.2 (0.1)	7.1 (0.1)	2.0 (0.2)
$\log K_{Na}^{Tl}$	6.2 (0.1)	3.6 (0.1)	1.2 (0.1)
$\log K_{K}^{Tl}$	2.9 (0.1)	0.5 (0.1)	0.5 (0.1)
$\log K_{NH_4}^{Tl}$	2.8 (0.3)	1.4 (0.1)	0.3 (0.1)
	Corresponding exchange selectivity coefficients for major cations		
$\log K_{Na}^{Ca}$	0.2 (0.1)	0.0 (0.1)	0.4 (0.2)
$\log K_{Na}^{NH_4}$	3.4 (0.3)	2.1 (0.1)	0.9 (0.1)
$\log K_{Na}^{K}$	3.3 (0.1)	3.0 (0.1)	0.7 (0.1)
	Cs-X and Rb-X exchange selectivity coefficients from ref. [35] [b]		
$\log K_{Na}^{Cs}$	7.0 (0.2)	3.6 (0.2)	1.6 (0.2)
$\log K_{Na}^{Rb}$	5.5 (0.2)[b]	2.8 (0.2)[b]	1.4 (0.2)[b]
$\log K_{K}^{Cs}$	4.6 (0.2)	1.5 (0.2)	0.5 (0.2)
$\log K_{K}^{Rb}$	2.2 (0.2)	0.5 (0.2)	0.5 (0.2)

[a]Site fractions from the generalised 3-site Cs^+ sorption model[35] were multiplied with the Tl-CEC of 0.260 eq/kg to obtain site concentrations.

[b]Rb^+-Na^+ selectivity coefficients were obtained by remodeling Rb^+-Na^+ cation exchange date from ref. [34] in the framework of the generalized 3-site sorption model as described for the corresponding Rb^+-K^+ selectivity coefficients in ref.[35].

626 **Table 2:** Comparison of the effective ionic radii (for 12-fold coordination), molar Gibbs
627 energies of ion hydration and Tl-X selectivity coefficients on FES and T2S for different cations
628 X.

Cation X	**Ionic radius**[a]	$\Delta G_{hydration}$[b]	$\log K_X^{Tl}$	
	(Å)	(kJ/mol)	FES	T2S
Ca^{2+}	1.34	-1505 (1205)	12.2	7.1
Na^+	1.39	-365 (65)	6.2	3.6
K^+	1.64	-295 (-5)	2.9	0.5
NH_4^+	1.67	-285 (-15)	2.8	1.4
Rb^+	1.72	-275 (-25)	0.7[c] (0.7)	0.8[c] (0)
Tl^+	1.70	-300	––	––
Cs^+	1.88	-250 (-50)	-0.8[c] (-1.7)	0[c] (-1.0)

629 [a]effective ionic radii for 12-fold coordinated cations from ref. [3] except for NH_4^+ from ref. [74]
630 [b]molar Gibbs energies of hydration from ref. [75]; Values in parentheses correspond to $\Delta G_{hydration, Tl} - \Delta G_{hydration, X}$.
632 [c]$\log K^{Tl}_{Rb}$ and $\log K^{Tl}_{Cs}$ calculated from $\log K^{Tl}_{Na}$, $\log K^{Rb}_{Na}$ and $\log K^{Cs}_{Na}$ from Table 1. Values in
633 parentheses were calculated from $\log K^{Tl}_{K}$, $\log K^{Rb}_{K}$, and $\log K^{Cs}_{K}$ and are considered less reliable.
634
635

Figures

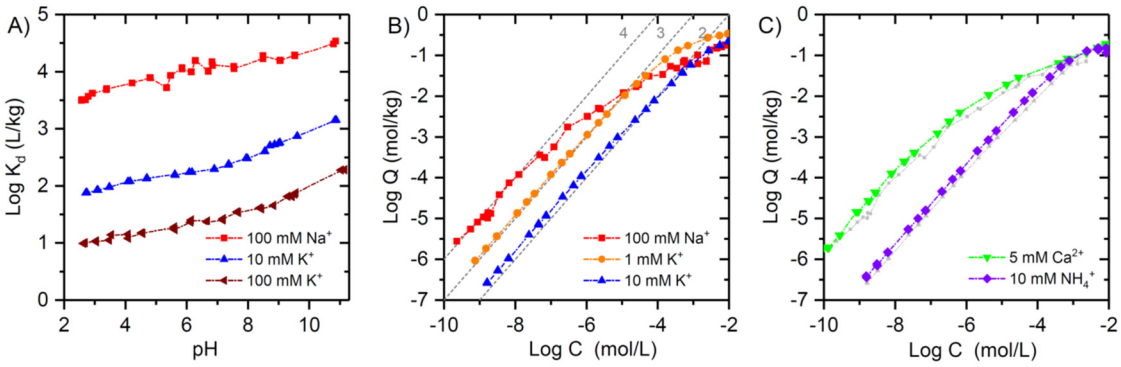

Figure 1. (A) Log K_d of trace Tl^+ adsorbed onto Na-illite (100 mM NaCl) and K-illite (10 and 100 mM KNO_3) from pH ~2.5 to ~11.0. (B) Adsorption isotherms for Tl^+ on illite at near neutral pH in 100 mM NaCl or $NaNO_3$, 1 mM and 10 mM KNO_3 electrolyte (diagonal gray dashed lines represent log K_d values of 4, 3 and 2 L/kg). (C) Adsorption isotherms for Tl^+ on illite at near neutral pH in 5 mM $Ca(NO_3)_2$ and 10 mM NH_4NO_3. Data for 100 mM Na^+ and 10 mM K^+ from panel B are shown in gray for comparison.

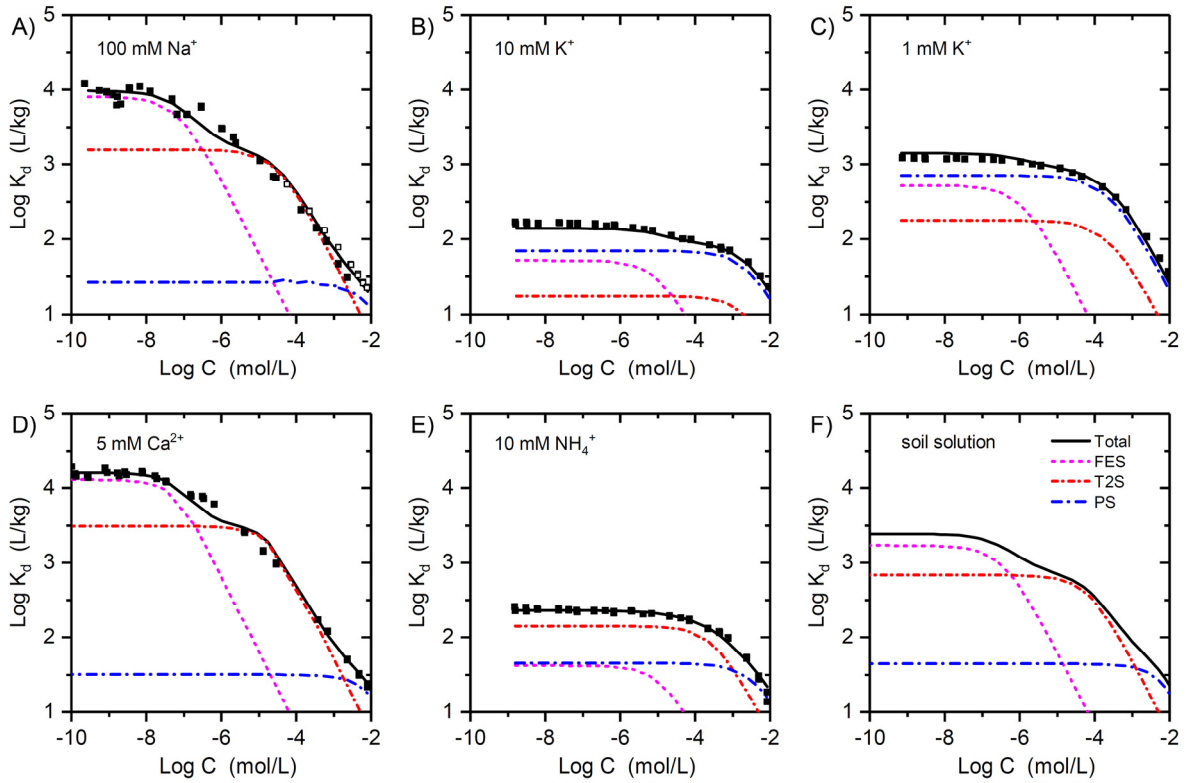

646

647 **Figure 2.** Log K_d (distribution coefficients) as a function of dissolved Tl^+ concentration for Tl^+
648 adsorption onto illite at near-neutral pH in (A) 100 mM NaCl (filled symbols) or $NaNO_3$,
649 (unfilled symbols) (B) 10 mM KNO_3, (C) 1 mM KNO_3, (D) 5 mM $Ca(NO_3)_2$, and (E) 10 mM
650 NH_4NO_3 (symbols). Model calculations (solid lines for total Tl^+ adsorption and broken colored
651 lines for Tl^+ adsorption on FES, T2S and PS) are based on parameters reported in Table 1. (F)
652 Calculated log K_d for Tl^+ adsorption onto illite in arable soil porewater with typical
653 concentrations of Ca^{2+} (2.00 mM), Mg^{2+} (0.46 mM), Na^+ (0.28 mM), K^+ (0.24 mM) and NH_4^+
654 (0.05 mM)[53] balanced by NO_3^- (see text for details).

655

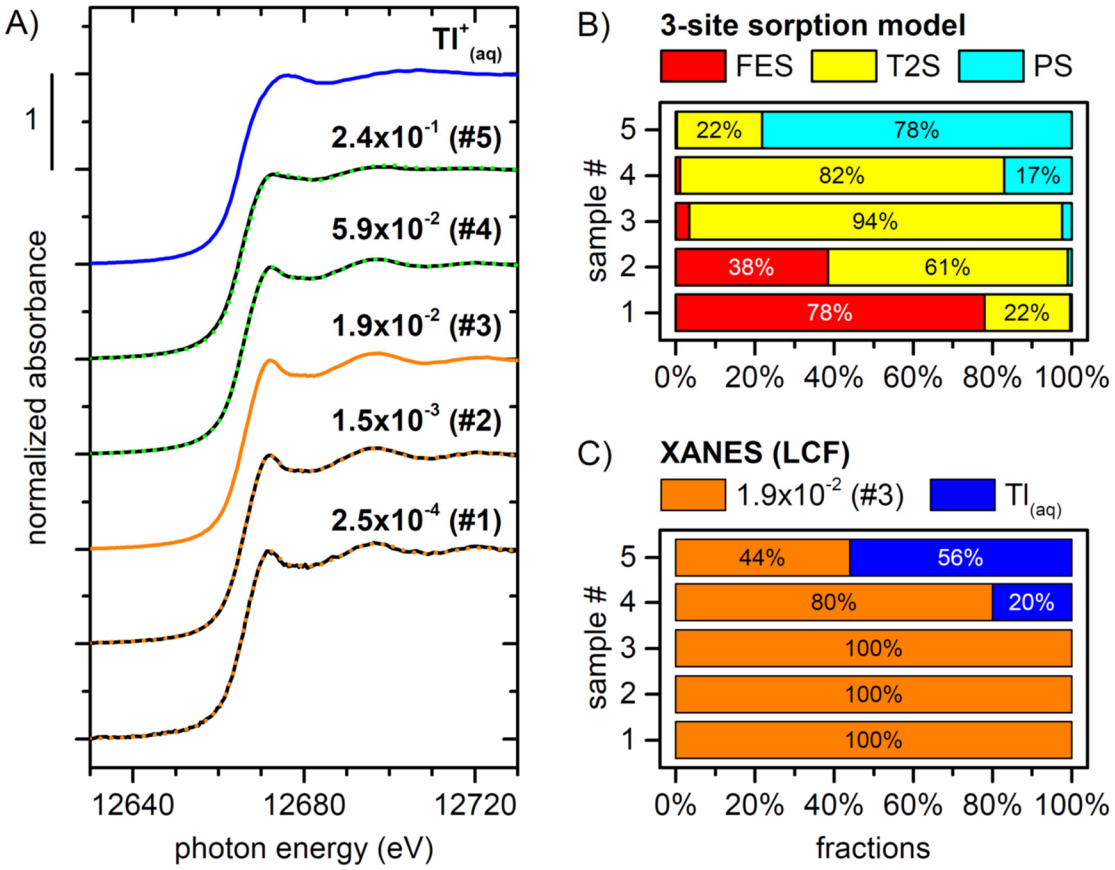

Figure 3. (A) Tl L_{III}-edge XANES spectra of Na-IdP with Tl^+ loadings from 2.5×10^{-4} to 2.4×10^{-1} mol/kg (50 to 49'000 mg/kg) (solid orange line for sample #3, solid black lines for other samples) and of aqueous Tl^+ (10 mM $TlNO_3$; solid blue line). (B) Calculated distribution of Tl over sorption model sites. (C) Fractions of spectra of sample #3 and aqueous Tl^+ used to reproduce the sample spectra #1 to #5 (reconstructions shown as short dashed green or orange lines in panel A).

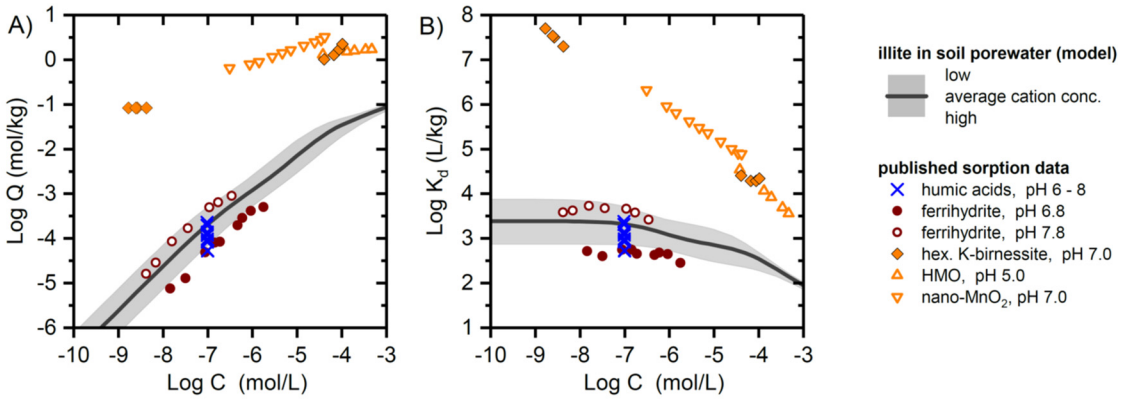

664

665 **Figure 4.** Modeled adsorption of Tl^+ onto illite in arable soil porewater (dark gray line; light
666 gray area) shown as log adsorbed amounts (A) and log distribution coefficients (B) compared
667 to published data (symbols) for Tl^+ adsorption onto two humic acids,[54] ferrihydrite[15] and three
668 hexagonal birnessites.[55-57] Model calculations were performed with parameters from Table 1
669 for average (dark gray line) as well as low and high concentrations of Ca^{2+}, Mg^{2+}, Na^+, K^+, and
670 NH_4^+ (light gray area) in arable soil porewater[53] (see text and Table S2 for details; average
671 concentrations: 2.00 mM Ca^{2+}, 0.46 mM Mg^{2+}, 0.28 mM Na^+, 0.24 mM K^+, 0.05 mM NH_4^+).
672 Published sorption data for two humic acids (in 100 mM $NaClO_4$),[54] ferrihydrite (in 10 mM
673 NaCl),[15] hexagonal K-birnessite (in 110 mM KNO_3),[57] hydrous manganese oxide (HMO),[55] and
674 nano-MnO_2 (in 2 mM MOPS)[56] (see SI for details on published sorption data).

675

676 **TOC Art**

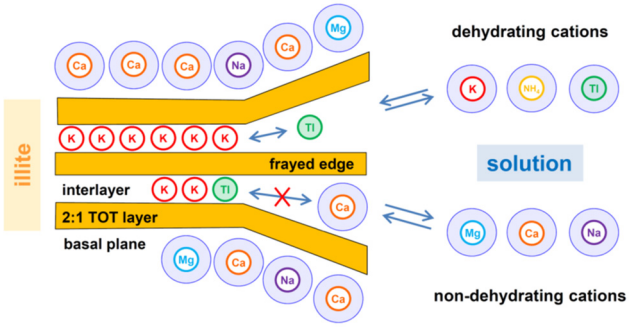

677

678

Supporting Information

Thallium Adsorption onto Illite

Silvan Wick[1,2], Bart Baeyens[3], Maria Marques Fernandes[3] and Andreas Voegelin[1*]

[1]Eawag, Swiss Federal Institute of Aquatic Science and Technology, Überlandstrasse 133, CH-8600 Dübendorf, Switzerland.

[2]Institute of Biogeochemistry and Pollutant Dynamics, ETH Zürich, CH-8092 Zürich, Switzerland.

[3]Paul Scherrer Institute, CH-5232 Villigen PSI, Switzerland.

[*]corresponding author, E-mail: andreas.voegelin@eawag.ch, phone: +41 58 765 54 70, fax: +41 58 765 58 02.

8 pages, 2 figures, 2 tables

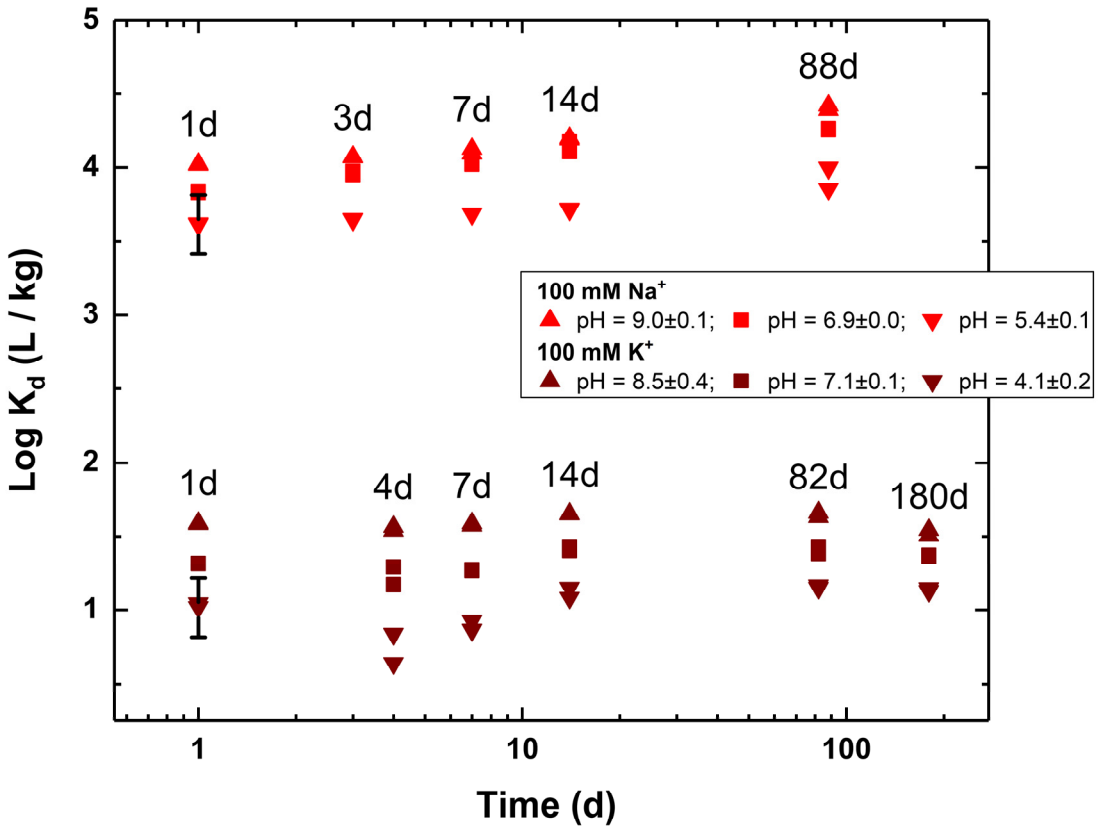

Figure S1. Kinetics of the adsorption of trace Tl^+ (total Tl concentration 10^{-8} M; illite concentration of 2.1 g/L) onto Na-IdP in 100 mM NaCl and onto K-IdP in 100 mM KNO_3 background electrolyte at three different pH values. Each treatment (Na-IdP or K-IdP; pH; time) was performed in duplicate.

In the 100 mM Na electrolyte, a slow increase in the log K_d values can be observed over time. This may indicate that rapid initial adsorption of Tl^+ onto illite is followed by slow fixation in the interlayer over time. The unsystematic temporal variations in the 100 mM K electrolyte are probably due to the experimental uncertainty (and potential outliers such as the samples at pH 4.1 after 4 days and pH 8.5 after 88 days) rather than a true temporal trend. The lack of a temporal trend may reflect that 100 mM K^+ effectively reduces Tl^+ adsorption at FES and subsequent diffusion into the interlayer.

Based on the results from the kinetic experiments, a reaction time of 14 d was considered suitable as a compromise between sufficient time for adsorption equilibration and limiting the relevance of ongoing fixation.

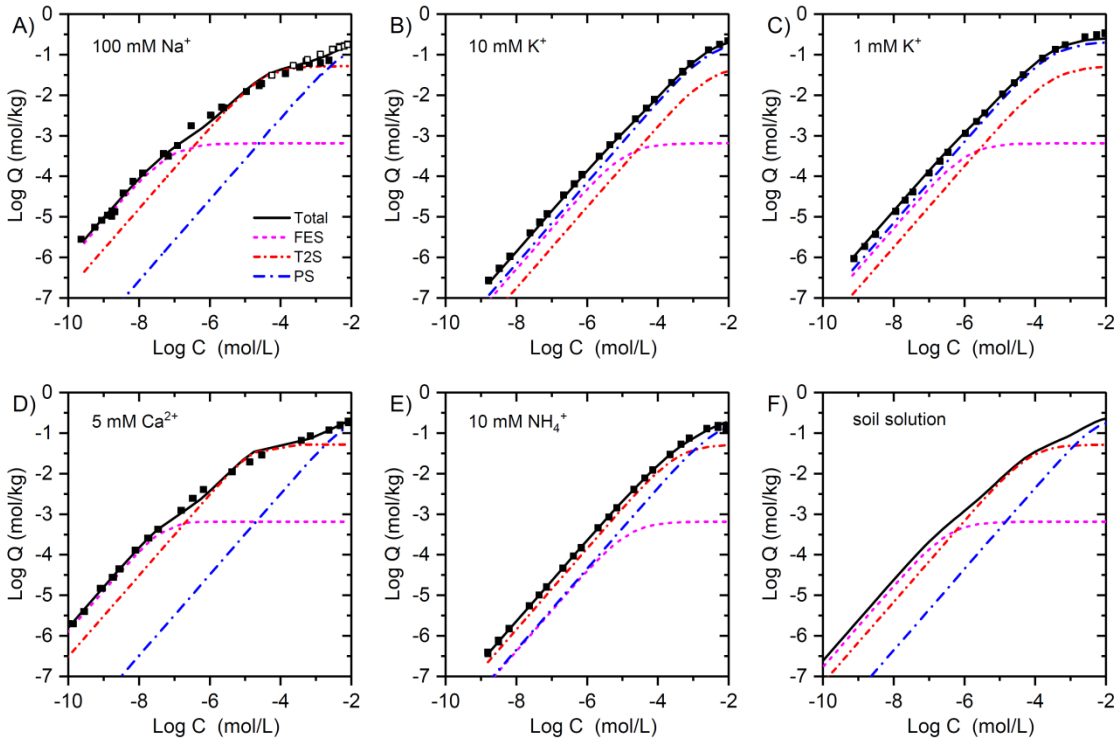

Figure S2. Experimental and modeled isotherms for Tl^+ adsorption onto illite at near-neutral pH in (A) 100 mM NaCl (filled symbols) or $NaNO_3$, (unfilled symbols) (B) 10 mM KNO_3, (C) 1 mM KNO_3, (D) 5 mM $Ca(NO_3)_2$, and (E) 10 mM NH_4NO_3 (symbols). Model calculations (solid lines for total Tl^+ adsorption and broken colored lines for Tl adsorption on FES, T2S and PS) are based on parameters reported in Table 1. (F) Calculated isotherm for Tl^+ adsorption onto illite in arable soil porewater with typical concentrations of Ca^{2+} (2.00 mM), Mg^{2+} (0.46 mM), Na^+ (0.28 mM), K^+ (0.24 mM) and NH_4^+ (0.05 mM) balanced by NO_3^- (see manuscript and Table S2 for details). Corresponding log K_d plots are shown in Figure 2 in the manuscript.

Table S1. Synopsis over experimental conditions in batch adsorption experiments.

Background electrolyte	pH[a]	Tl (mol/L)[b]	illite (g/L)	pH buffer[a]
pH-dependent sorption experiments				
100 mM NaCl	~2.5 - ~11.0	10^{-8}	2.0	HNO_3, organic buffers, NaOH
100 mM KNO_3	~2.5 - ~11.0	10^{-8}	2.1	HNO_3, organic buffers, NaOH
10 mM KNO_3	~2.5 - ~11.0	10^{-8}	2.1	HNO_3, organic buffers, NaOH
Concentration-dependent adsorption isotherms				
100 mM NaCl	6.2 ± 0.1	$\sim10^{-10}$ – $\sim10^{-7}$ $\sim10^{-7}$ – $\sim10^{-5}$ $\sim10^{-5}$ – $\sim10^{-3}$	0.7 1.5 3.6	illite illite illite
100 mM $NaNO_3$	6.4 ± 0.1	$\sim10^{-4}$ – $\sim10^{-2}$	3.8	illite
1 mM KNO_3	6.5 ± 0.2	$\sim10^{-10}$ – $\sim10^{-2}$	1.7	illite
10 mM KNO_3	6.5 ± 0.1	$\sim10^{-9}$ – $\sim10^{-2}$	2.6	illite
5 mM $Ca(NO_3)_2$	6.4 ± 0.1	$\sim10^{-11}$ – $\sim10^{-2}$	2.0	illite
10 mM NH_4NO_3	6.8 ± 0.1	$\sim10^{-9}$ – $\sim10^{-2}$	1.2	illite

[a]see Materials and Methods for details on pH adjustment in pH-dependent experiments; in the concentration-dependent experiments, the pH was buffered by the illite and the measured pH after equilibration is given (average ± standard deviation).
[b]concentration of total Tl in pH-dependent experiments and of final dissolved Tl in concentration-dependent experiments.

Table S2. Lower and upper bound of frequent concentrations of Ca^{2+}, Mg^{2+}, Na^{+}, K^{+} and NH_4^{+} in porewater of arable soils (from ref. 1) and resulting average concentrations derived on log-scale. LOG: values of concentrations in [mmol/L]. Cation concentrations were balanced by NO_3^{-} for calculations with the adsorption model.

	Range of frequency concentrations					
	Lower bound		**Upper bound**		**Average**	
	(mmol/L)	LOG	(mmol/L)	LOG	(mmol/L)	LOG[a]
Ca^{2+}	1.00	0.00	3.99	0.60	2.00	0.30
Mg^{2+}	0.21	-0.69	1.03	0.01	0.46	-0.34
Na^{+}	0.09	-1.06	0.87	-0.06	0.28	-0.56
K^{+}	0.08	-1.12	0.77	-0.12	0.24	-0.62
NH_4^{+}	0.01	-1.95	0.22	-0.65	0.05	-1.30
NO_3^{-} [b]	2.58	–––	11.9	–––	5.48	–––

[a]Average of LOG transformed lower and upper bound concentrations.

[b]NO_3^{-} calculation calculated to charge balance cation concentrations.

Derivation of published data for Tl adsorption onto different adsorbents shown in Fig. 4

Tl^+ adsorption onto humic acids

Data on the adsorption of Tl^+ by two purified humic acids was derived from a study by Liu et al. (2011).[2] In this study, the adsorption of Tl^+ was examined in 100 mM $NaClO_4$ electrolyte containing 20 mg/L humic acid and 10^{-7} M total Tl^+ at pH values from 4 to 8 after an equilibration period of 48 h.

Log K_d values were digitized from Fig. 3 in Liu et al. (2011) and the information on the concentration of total Tl and humic acid in solution was used to calculate the logarithm of the dissolved concentration and adsorbed amount of Tl^+. Only results obtained at pH values from 6 to 8 are shown in Fig. 4 in our manuscript.

Tl^+ adsorption onto ferrihydrite

Data on the adsorption of Tl^+ onto ferrihydrite was derived from a study by Casiot et al. (2011).[3] In this study, the adsorption of Tl^+ onto freshly synthesized (<10 days; no drying) two-line ferrihydrite was examined in 10 mM $NaNO_3$ solution at pH values of 6.8 and 7.8 for total Tl^+ concentrations from ~2.5×10^{-9} to 1.5×10^{-6} M. Data for dissolved and adsorbed Tl^+ from adsorption isotherms at pH 6.8 and 7.8 were digitized from Fig. 3 in the article by Casiot et al. (2011) and used to calculate the resulting log K_d.

Tl^+ uptake by hexagonal K-birnessite

Data on the uptake of Tl^+ by poorly-crystalline hexagonal K-birnessite was derived from a study by Nielsen et al. (2013).[4] The synthesis protocol followed in this study (reaction of permanganate with hydrochloric acid) results in poorly-crystalline hexagonal K-birnessite.[4] Fresh birnessite suspensions were used for the experiments.

A first sorption experiment at high Tl loadings (4 samples; Tl-25-1 to Tl-25-4; Tables 1 and 2 in Nielsen et al. (2013)) was performed at 25°C over an equilibration time of 48 h in 110 mM KNO_3 at pH ~7 at a total Tl concentration of ~1.2×10^{-4} M at four different birnessite concentrations (~80, 40, 20, 10 mg/L). Final dissolved concentrations and adsorbed amounts of Tl were derived from Table 2 in Nielsen et al. (2013).

A second sorption experiment at low Tl loadings (4 samples; LowTl-2201, LowTl-2202, LowTl-2203, LowTl-2204; Tables 1 and 3 in Nielsen et al. (2013)) was performed at 22°C over an equilibration time of 44 h in 110 mM KNO_3 at pH ~7 at four total Tl concentrations (2.3×10^{-6} to 7.4×10^{-7} M) and birnessite concentrations (~26 to 8.8 mg/L) (i.e., at constant total Tl/birnessite ratio). Final dissolved concentrations and adsorbed amounts of Tl were derived from Table 3 in Nielsen et al. (2013).

Nielsen et al. (2013) interpreted the decreasing Tl isotope fractionation with increasing Tl loading of the hexagonal birnessite as an indication for the decreasing importance of oxidative Tl scavenging once the capacity of vacancy sites was exceeded.[4]

Tl^+ uptake by hydrous manganese oxide (HMO)

Data on the uptake of Tl^+ by hydrous manganese oxide (HMO) was derived from a study by Wan et al. (2014).[5] The XRD pattern of the HMO, synthesized by reaction of dissolved $MnSO_4$ with NaOCl, resembles the pattern of poorly crystalline hexagonal birnessite (delta-MnO_2).[5] Dried HMO was used for the experiments.

Data from an adsorption experiment with 50 mg/L HMO in water at pH 5.0 and 30°C (with dissolved Tl up to ~4.7×10^{-4} M) was digitized from Fig. 6 in Wan et al. (2014). From the dissolved concentrations and sorbed amounts of Tl, the log K_d values were derived.

XPS results suggested that Tl^+ uptake at slightly acidic to neutral pH was predominantly due to Tl^+ adsorption at the employed Tl loadings, whereas oxidative scavenging was more relevant at acidic pH (~55% Tl(III) on HMO at pH 2.0).[5]

Tl^+ uptake by nano-MnO_2

Data on the uptake of Tl^+ by nano-MnO_2 was derived from a study by Huangfu et al. (2015).[6] The nano-MnO_2 was produced by reduction of $KMnO_4$ with NaS_2O_3. The solid phase Mn has an average oxidation state of 4.0 and the particles are ~56 nm in size.[6] Based on synthesis conditions, the oxidation state and particle size of the product, and the XRD pattern of nano-MnO_2 reported in the supporting information of an earlier article by the same research group,[7] the synthesis product is assumed to correspond to hexagonal delta-MnO_2. For the sorption experiments, fresh nano-MnO_2 suspensions (stored less than 2 weeks at 4°C) were used.

Sorption experiments were performed at 25°C in 2 mM MOPS buffer adjusted to pH 7.0. After addition of Tl^+ at various levels, an aliquot of suspended n-MnO_2 was added corresponding to 50 mM MnO_2 (~4.3 g/L MnO_2). The reaction time was 2 h. The adsorbed amounts and dissolved concentrations from an adsorption isotherm at pH 7.0 were digitized from Fig. 2, and the log K_d was calculated from the respective values.

Based on the observation of dissolved Mn release and nano-MnO_2 aggregation in sorption experiments at pH 4.0 but not in experiments at pH 7.0, it was suggested that Tl uptake at the lower pH was (partially) due to oxidation, whereas uptake at pH 7.0 was considered to be mainly due to adsorption of Tl^+.[6]

References

1. Blume, H. P.; Scheffer, F.; Schachtschabel, P., *Scheffer/Schachtschabel Soil Science*. Springer Verlag: Berlin, Heidelberg, 2016; p 618.
2. Liu, J.; Lippold, H.; Wang, J.; Lippmann-Pipke, J.; Chen, Y., Sorption of thallium(I) onto geological materials: Influence of pH and humic matter. *Chemosphere* **2011,** *82*, 866-871.
3. Casiot, C.; Egal, M.; Bruneel, O.; Verma, N.; Parmentier, M.; Elbaz-Poulichet, F., Predominance of aqueous Tl(I) species in the river system downstream from the abandoned Carnoulès mine (Southern France). *Environ. Sci. Technol.* **2011,** *45*, 2056-2064.
4. Nielsen, S. G.; Wasylenki, L. E.; Rehkämper, M.; Peacock, C. L.; Xue, Z.; Moon, E. M., Towards an understanding of thallium isotope fractionation during adsorption to manganese oxide. *Geochim. Cosmochim. Acta* **2013,** *117*, 252-265.
5. Wan, S.; Ma, M.; Lv, L.; Qian, L.; Xiu, S.; Xue, Y.; Ma, Z., Selective capture of thallium(I) ion from aqueous solutions by amorphous hydrous manganese dioxide. *Chemical Engineering Journal* **2014,** *239*, 200-206.
6. Huangfu, X.; Jiang, J.; Lu, X.; Wang, Y.; Liu, Y.; Pang, S.-Y.; Cheng, H.; Zhang, X. H.; Ma, J., Adsorption and oxidation of thallium(I) by a nanosized manganese dioxide. *Water Air and Soil Pollution* **2015,** *226*, 2272:1-9.
7. Jiang, J.; Pang, S.-Y.; Ma, J., Oxidation of triclosan by permanganate (Mn(VII)): Importance of ligands and in situ formed manganese oxides. *Environ. Sci. Technol.* **2009,** *43*, 8326–8331.